Clays and Clay Minerals, Vol. 56, No. 6, 693–710, 2008.

CLAY MINERALOGY OF THE CENTRAL NORTH SEA UPPER CRETACEOUS–TERTIARY CHALK AND THE FORMATION OF CLAY-RICH LAYERS

HOLGER LINDGREEN[1,*], VICTOR A. DRITS[2], FINN C. JAKOBSEN[1], AND BORIS A. SAKHAROV[2]

[1] Geological Survey of Denmark and Greenland, Øster Voldgade 10, DK-1350 Copenhagen K, Denmark
[2] Geological Institute, Russian Academy of Science, Pyzhevsky per D7, 119017 Moscow, Russia

Abstract—Upper Cretaceous–Danian chalk and interbedded clay-rich layers from wells of the South Arne Field and adjacent wells in the North Sea and from Stevns in Zealand have been investigated to determine the clay mineralogy in the chalk and the origin of the interbedded clay-rich layers. The mineralogy, with emphasis on clay mineralogy, was determined after removal of the calcite by dissolution at pH 4.5–5 in order to preserve the other minerals. Generally, mixed-layer minerals are the dominant clay minerals, except for two wells, Rigs-1 and Rigs-2, where a 3D ordered kaolinite prevails. A detailed structural characterization of the mixed-layer minerals was carried out by modeling of the X-ray diffraction (XRD) patterns. In most of the samples dominated by mixed-layer minerals, two mixed-layer phases, a high-smectite illite-smectite (I-S) and a low-smectite illite-smectite-chlorite (I-S-Ch), prevail, irrespective of depth or location of the samples. However, some samples contain I-S-Ch and ordered S-Ch, and others a chlorite-serpentine (Ch-Sr) phase, and these samples probably formed during diagenesis at higher temperatures. The clay-rich layers and the adjacent chalk have the same or quite similar clay mineralogy, both with respect to kaolinite *vs*. mixed-layer minerals and with respect to their detailed structure. In conclusion, the kaolinite is detrital and the I-S minerals formed in the chalk from volcanic ash. The main conclusion is that the clay-rich layers in the North Sea chalk formed by dissolution of the calcite in the chalk and that this dissolution took place at burial depths of >1 km, probably through migration of solutions through permeable chalk layers.

Key Words—Chalk, Chlorite-smectite, Clay Layers, Cretaceous, Danian, Diagenesis, Illite-smectite, Kaolinite, North Sea, Seams, XRD.

INTRODUCTION

The Late Cretaceous–Danian chalk is a most important reservoir in the oil fields in the North Sea. The chalk consists of low-Mg-calcite coccolithic debris, foraminifera, shell debris, sponge spicules, and radiolaria and is interbedded with clay-rich horizons. In the chalk, the layer silicates usually comprise <10% of the chalk and, consequently, most investigations on chalk diagenesis have focused on carbonate mineralogy. For the North Sea Upper Cretaceous–Danian chalk, several oil well samples were found (Lindgreen *et al*., 2002) in which smectitic minerals dominate the layer silicates of both the chalk and the interbedded clay-rich layers. The clay minerals of the pre-Campanian, Upper Cretaceous chalks of England and Ireland (Jeans, 1968, 2006; Jeans *et al.*, 1982) and of northern France (Deconinck and Chamley, 1995) are mainly smectites which have been associated with the warm, humid climate and the high sea level prevailing during this period, resulting in deposition of pedogenic Fe-rich smectites and, with deposition of volcanic ash in the sea, resulting in the formation of Mg-rich smectites (Deconinck and Chamley, 1995; Deconinck *et al*., 2005; Jeans, 2006). The smectitic minerals in the Upper Cretaceous–Danian Chalk of the North Sea were recently demonstrated to be a multiphase mixture of illite-smectite (I-S) and illite-smectite-chlorite (I-S-Ch) (Lindgreen *et al.*, 2002). This mixture probably formed from volcanic ash through an intermediate mixture of two I-S phases (Drits *et al.*, 2004). The appearance and distribution of the clay-rich horizons vary throughout the chalk succession and their origin and composition have been the subject of several investigations (Garrison and Kennedy, 1977; D'Heur, 1984; Wray, 1995, 1999; Davison *et al*., 2000; Safaricz and Davison, 2005; Simonsen and Toft, 2006). In the smectite-bearing Upper Cretaceous chalk, the clay-rich horizons usually have a smectitic clay mineralogy and have been described as solution seams and flaser structures formed during late burial diagenesis (pressure solution and compaction) of the chalk (Garrison and Kennedy, 1977; D'Heur, 1984; Davison *et al*., 2000; Safaricz and Davison, 2005), probably taking place in chalk layers having a greater primary clay minerals content (Garrison and Kennedy, 1977). Alternatively, the clay-rich horizons have been proposed to represent periods of intense volcanic ashfalls (Wray, 1995, 1999; Simonsen and Toft, 2006). For Turonian chalks, Wray

* E-mail address of corresponding author:
hl@geus.dk
DOI: 10.1346/CCMN.2008.0560610

(1999) used the 001 peak area ratio for smectite and illite to compare clay-rich beds and adjacent white chalk and found that three beds had low ratios, being close to those of the adjacent chalk, whereas five beds with greater ratios had adjacent chalk with low ratios. Wray (1999) concluded from the different mineralogy of the five clay-rich beds with the high ratios and the adjacent chalk and from rare-earth elemental compositions that these beds were bentonites formed from volcanic ashfalls.

Kaolinite is usually associated with continental weathering in a neutral to weakly acid environment or to diagenetic formation in sandstones (Millot, 1970) and, when found in the chalk, is normally attributed to detrital input from local exposed highs and platform margins (Thiry and Jacquin, 1993; Deconinck and Chamley, 1995; Deconinck *et al.*, 2005; Jeans, 2006). Whereas smectitic minerals prevail in the Upper Cretaceous–Danian chalk in the North Sea, kaolinite is reported to be present locally, *e.g.* in the Eldfisk field (Maliva *et al*., 1999).

A prevalent 3D crystalline kaolinite was found by the present authors in the chalk matrix and clay-rich horizons throughout the Maastrichtian–Danian section in two wells (Rigs-1 and Rigs-2) in the South Arne Field in the Danish North Sea (Figure 1), whereas smectitic minerals prevailed in this chalk section from the other wells drilled in the field (Baron-2, SA-1 and I-1) and the surrounding area. The origin and diagenesis of the clay minerals and the mechanism for formation of the clay-rich layers are discussed below in relation to these findings.

MATERIALS

In a previous investigation on North Sea chalk, samples were taken from the Santonian–Danian in wells Baron-2 and I-1 from the South Arne Field and in the wells West Lulu-1 and Mona-1 in adjacent fields (Lindgreen *et al.*, 2002). Samples from the K/T boundary and the Maastrichtian gray chalk below were investigated from a location south of Højerup Old Church at Stevns Klint, Sjælland, Denmark (Drits *et al.*, 2004).

Samples from the Maastrichtian–Danian from the South Arne Field (wells SA-1, Rigs-1 and -2, and additional samples from the wells Baron-2 and I-1), from well Q-1, and from wells T-1 and Otto-1 of the Svend Field to the north of the South Arne Field (Figure 1) were included in the present study. In addition, Lower Cretaceous samples from the Valdemar 2 well in the Valdemar Field were investigated. All samples were core samples. Essentially, all clay-rich layers of the cores were sampled together with the adjacent chalk (Table 1). The clay-rich layers were horizontal or sub-horizontal and, when compared to the descriptions of Garrison and Kennedy (1977), were generally of the composite solution-seam type (*e.g.* the layers in Rigs 1 (Figure 2a) and the layer in Baron 2859.09 m (Figure 2b)), but occasional flaser structures (*e.g.* Baron 2859.92 m, Figure 2b) or nodular flaser chalk were also found (SA-1, 3410.6 m, Figure 2c).

METHODS

Chemical pre-treatment

The large amounts of calcite in chalk were removed by dissolution procedures prior to mineralogical investigation of the non-calcite minerals, which constituted <20% of the total sample for the Upper Cretaceous samples, but more than that for many Danian samples (Table 1). The chalk samples were crushed to pass a 4 mm sieve. The samples were then added to 200 mL of distilled water, and the calcite was removed in a solution buffered at pH 4.5–5 with acetic acid to minimize the degradation of other minerals (dolomite, quartz, and clay minerals, especially chlorite). The supernatant was removed by centrifugation and the residues air-dried. The chalk residues and the clay-rich layer samples were dispersed ultrasonically and the clay fraction (<2 μm) was obtained by centrifugation.

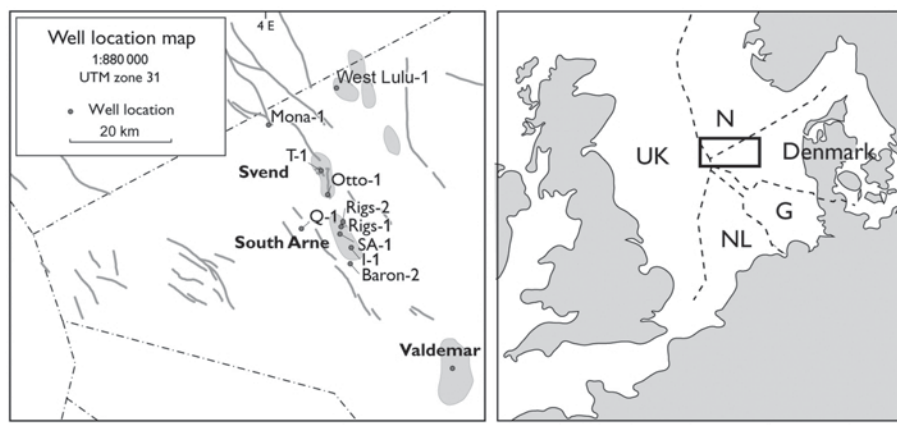

Figure 1. Location map.

Isolation of mixed layers

For samples where the mixed-layer phase was dominant, the mixed-layer fraction was isolated by centrifugation (Hansen and Lindgreen, 1989), yielding particles predominantly <500 Å in diameter and <100 Å thick. This fraction contained <15% discrete minerals, which made it suitable for the study of mixed-layer minerals.

X-ray diffraction

The mixed-layer fraction was saturated with K^+ and Mg^{2+} by five repeated washings using 1 M chloride solutions. Oriented specimens were prepared from ultrasonically dispersed suspensions by the pipette method using 2.5 mg/cm^2 of specimen. Mg-saturated specimens were analyzed having been air-dried and after glycolation for 3 days at 60ºC in ethylene-glycol vapor. K-saturated specimens were analyzed in dry N_2 gas after heating to 150ºC for 1 h. For selected samples, non-fractionated residues were dispersed for 15 min using ultrasonic treatment. K- and Mg-saturated and oriented specimens were analyzed after air-drying.

The XRD patterns were obtained using CoKα radiation with Philips PW1050 and PW3040 diffractometers. The Philips PW1050 device had a vertical goniometer supplied with two Fe filters and a normal focus tube. The PW3040 device had a vertical goniometer with a curved graphite monochromator and a fine-focus tube. For randomly oriented specimens, 1º fixed divergence and anti-scatter slits were used and intensities were measured for 10 s per 0.1º2θ step, but for selected kaolinitic samples, intensities were measured for 40 s per 0.02º2θ step. For oriented specimens, 1/4º fixed divergence and anti-scatter slits were used and intensities were measured for 10 s per 0.1º2θ step in the interval 1.5−65º2θ.

Thermal analysis (DTA-EGA)

A Stanton-Redcroft DTA 673-674 with gas outlet to non-dispersive infrared H_2O and CO_2 detectors was used to quantify the amounts of H_2O and CO_2 released during heating (Morgan, 1977). Samples were heated in a flow of 400 mL/min of 40% O_2 in N_2. From the amount and pattern of release of CO_2 the amount of non-dissolved carbonates (dolomite and/or ankerite) in the residues was determined.

INTERPRETATIONS

Simulation of the XRD patterns of mixed-layer minerals

In order to simulate the XRD patterns for oriented samples, the program of Drits and Sakharov (1976) was used. Corrections for instrumental variables such as horizontal and vertical beam divergences, goniometer radius, and dimensions and thickness of samples were carried out according to the recommendations of Reynolds (1986) and Drits *et al*. (1993).

In the following, I, S, V, Ch, and Sr denote illite, smectite, vermiculite, chlorite, and serpentine-like interlayers or layers, respectively. I-S is a mixed-layer illite-smectite; S-Ch, a mixed-layer smectite-chlorite; I-S-Ch, a mixed-layer illite-smectite-chlorite; I-S-V, a mixed-layer illite-smectite-vermiculite; and Ch-Sr a mixed-layer chlorite-serpentine. LS and HS are low-smectite and high-smectite mixed-layer phases, respectively. Expandable layers are defined as smectite and vermiculite if, in the glycolated state, their interlayers contain two or one layers of glycol molecules, respectively, independent of the nature of the exchangeable cations.

For structural models of air-dried and glycolated I-S containing Mg cations in the expandable interlayers, the *z* coordinates and site occupancies for 2:1 layers and interlayers of Moore and Reynolds (1989) were used. The K content in illite interlayers was 0.75 atoms per $O_{10}(OH)_2$. K cations were placed in the center of mica interlayers and the thickness of illite layers was set to 9.98 Å. In accordance with chemical analysis (Lindgreen *et al*., 2002) the chlorite structural unit in mixed-layer I-S-Ch and S-Ch was assumed to consist of a dioctahedral 2:1 layer and a trioctahedral brucite-like sheet. Thicknesses of coherent scattering domains (CSDs) were log-normally distributed and the parameters of this distribution were determined using a mean thickness of CSDs and the regression given by Drits *et al.* (1997) with mean and maximum thicknesses of CSDs as variable parameters. Agreement between calculated and experimental XRD patterns was obtained in the present study, not only for positions but also for the intensity and profiles of the reflections. Furthermore, such agreement was obtained for one structural model applied to the different XRD patterns corresponding to different treatments of each sample. This approach allows determination of structural and probability parameters for each of the coexisting mixed-layer varieties and their relative weight content.

RESULTS

Non-clay minerals

For most samples, most of the residue consisted of quartz (Table 1). The amount of residue was large (6−35%) in the Danian chalk and small (1−7%) in the Maastrichtian chalk. For both the Danian and Maastrichtian samples, the residue quartz consists mainly of spheres of ~500 Å in diameter (Jakobsen *et al.*, 2000). In some residues, an occasional carbonate was present, which in XRD resembled ankerite, with one dominant, sharp peak at 2.89 Å, but the DTA-EGA had one or two peaks at 750−900ºC, and therefore was a dolomite (Webb and Krüger, 1970). This dolomite was present in significant amounts in the Maastrichtian of well SA-1 and in some of the Danian−Maastrichtian samples of well Rigs-1 (Table 1).

Table 1a. Upper Cretaceous–Danian samples with mixed-layers as the dominant clay mineral phase. Amount (wt.%) of insoluble residues, dolomite, and quartz.

Sample	Well	Depth (m)	Age	Type	Residue (%)*	Dolomite (%)*	Quartz (%)*
I9106R	I-1	2775.5	Danian	Chalk	6		5
I9149R	I-1	2788.8	Danian	Chalk	19		3
I9190R	I-1	2801.1	Maastrichtian	Chalk	6		2
I9192R	I-1	2801.7	Maastrichtian	Chalk	11		3
I9203L	I-1	2805.1	Maastrichtian	Clay layer	68		11
I9218R	I-1	2809.6	Maastrichtian	Chalk	7		2
L9445R	West Lulu1	2878.8	Danian	Chalk	18		9
M10446R	Mona 1	3183.9	Maastrichtian	Chalk	2		1
M10448R	Mona 1	3184.6	Maastrichtian	Chalk	2		1
M10470R	Mona 1	3191.3	Maastrichtian	Chalk	3	(tr.)	1
HSI	Stevns	Outcrop	D/M boundary	Clay layer			
GRI	Stevns	Outcrop	Maastrichtian	Chalk			
B2849L	Baron-2	2849.2	Danian	Clay layer	42		6
B2849R	Baron-2	2849.3	Danian	Chalk	28		14
B2853R	Baron-2	2853.7	Danian	Chalk	12		4
B2855L	Baron-2	2855.3	Danian	Clay layer	66		4
B2857R	Baron-2	2857.3	Danian	Chalk	31		3
B2859.0L	Baron-2	2859.09	Danian	Clay layer	39		7
B2859L	Baron-2	2859.4	Danian	Clay layer	34		16
B2859R	Baron-2	2859.70	Danian	Chalk	31		19
B2860L	Baron-2	2859.92	Danian	Clay layer	39		13
B2859R	Baron-2	2859.99	Danian	Chalk	24		18
B2860R	Baron-2	2860.1	Danian	Chalk	19		4
B2863aR	Baron-2	2863.3	Danian	Chalk (green)	38		3
B2863bR	Baron-2	2863.3	Danian	Chalk (white)	42		13
B2864R	Baron-2	2863.6	Danian	Chalk	13		7
B2865L	Baron-2	2864.6	Danian	Clay layer	36		14
B2867R	Baron-2	2866.83	Danian	Chalk	21		6
B2870L	Baron-2	2870.8	Danian	Clay layer	55		4
B2872L	Baron-2	2872.8	Danian	Clay layer	48		4
B2873R	Baron-2	2873.1	Danian	Chalk	14		5
B2876R	Baron-2	2876.2	Danian	Chalk	22		12
B2885L	Baron-2	2885.3	Danian (Camp?)	Clay layer			1.0
B2886R	Baron-2	2886.8	Campanian	Chalk	2		0.2
B2895L	Baron-2	2895.6	Campanian	Clay layer			
B2895R	Baron-2	2895.6	Campanian	Chalk	4		1
B2900R	Baron-2	2900.9	Campanian	Chalk	4		1
B2908L	Baron-2	2908.9	Santonian	Clay layer			5.9
B2919L	Baron-2	2919.9	Santonian	Clay layer			5.4
B2926R	Baron-2	2926.1	Santonian	Chalk	19		11
Q10133R	Q-1	3088.5	Danian	Chalk	30		24
T7269R	T-1	2215.6	Danian	Chalk	30		1
T7349R	T-1	2240.0	Danian	Chalk	22		8
T7398L	T-1	2254.9	Danian	Clay layer	39		8
T7491R	T-1	2283.3	U. Maastrichtian	Chalk	2		0.4
T7512R	T-1	2289.7	U. Maastrichtian	Chalk	2		0.4
T7618L	T-1	2322.0	L. Maastrichtian	Clay layer	50		15
T7621L	T-1	2322.9	L. Maastrichtian	Clay layer	52		7
O8117R	Otto-1	2474.1	Danian	Chalk	49		32
O8135L	Otto-1	2479.5	Danian	Clay layer	58		14
O8152R	Otto-1	2484.7	D/M boundary	Chalk	7		3
S3317.1R	SA-1	3317.15	Danian	Chalk	17		12
S3317.9R	SA-1	3317.94	Danian	Chalk	19		12
S3331L	SA-1	3331.50	Danian	Clay layer	32		11
S3344R	SA-1	3344.15	Danian	Chalk	35		35
S3349R	SA-1	3349.46	Danian	Chalk	30	(tr.)	(30)
S3352L	SA-1	3352.59	Danian	Clay layer	51		6.0
S3353L	SA-1	3353.00	Danian	Chalk	54		54
S3380R	SA-1	3380.03	Maastrichtian	Chalk	4	0.74	1.4
S3396R	SA-1	3396.74	Maastrichtian	Chalk	2	0.28	0.7
S3410R	SA-1	3410.56	Maastrichtian	Chalk	7	3.9	1.8
S3410L	SA-1	3410.56	Maastrichtian	Clay layer	51	34	11
S3437R	SA-1	3437.79	Maastrichtian	Chalk	2	0.33	0.5

Note: R and L denote samples of chalk and clay-rich layers, respectively.
*: % of total sample

Table 1b. Samples with kaolinite as the dominant clay phase. Amount (wt.%) of insoluble residues, dolomite, kaolinite, and quartz.

Well	Sample	Age	Type	Residue (%)	Dolomite (%)	Kaolinite (%)	Quartz (%)
Rigs-1	2794.3 m	Danian	Chalk	100			100
	2801.3 m	Danian	Chalk	31	0.9	17	9
	2802.9 m	Danian	Chalk	26			21
	2804.7 ma*	Danian	Chalk	22		4	18
	2804.7 mb**	Danian	Chalk	27		5	19
	2822.7 m	Danian	Clay layer	45	10	23	6
	2823.3 m	Danian	Chalk + clay	29	1.5	7	12
	2824.3 m	Danian	Chalk + clay	30		8	19
	2827.6 m	Danian	Clay layer	56	6	7	38
	2828.3 m	Danian	Clay layer			40	18
	2829.4 m	Danian?	Chalk	10		2	8
	2838.9 m	Danian?	Chalk	3			1
	2942.9 m	Maastrichtian	Chalk	4			1
	2849.9 m	Maastrichtian	Chalk	3	0.7		1
	2849.9 m	Maastrichtian	Clay layer	60	15		10
Rigs-2	2797.65 m	Danian	Chalk	35	0.7	5	19
	2804.00 m	Danian	Clay layer		(tr.)	20	3
	2812.10 m	Danian	Chalk	11	(tr.)	1	6
	2825.65 m	Danian	Clay layer			10	14
	2828.40 m	Danian	Chalk	6		1	4
	2829.60 m	Danian	Clay layer			85	2
	2838.75 m	Maastrichtian	Chalk + clay	8		1	1
	2839.60 ma*	Maastrichtian	Chalk	3		1	1
	2839.60 mb**	Maastrichtian	Chalk	4		1	1
	2856.40 m	Maastrichtian	Chalk	1	(tr.)	1	0.3
	2863 m	Maas/Aptian	Clay layer			15	5
	2866 m	Aptian	Clay layer			12	10
Valdemar-2	2281.4 m	Aptian	Chalk	47		40	4
	2281.4 m	Aptian	Clay layer	68			

* visually clay-poor chalk
** visually clay-rich chalk

Clay mineralogy

From the clay mineralogy, the Upper Cretaceous–Danian samples could be divided into two groups.

Group 1 includes the samples from the wells I-1, Baron-2, and SA-1 in the South Arne Field, plus the samples from wells T-1 and Otto-1 from the Svend Field, from wells Q-1 (one sample), West Lulu-1 (one sample), Mona-1 (three samples), and from the outcrop at Stevns (two samples). They are dominated by 2:1 layer minerals having a 14–15 Å peak in Mg-saturated and air-dried specimens and contain small amounts of illite and kaolinite (Figure 3a,b). The dominant 2:1 layer minerals are in fact a mixture of at least two phases, I-S and I-S-Ch (or -V) (Lindgreen *et al*., 2002; Drits *et al*., 2004).

Group 2 includes the samples (Danian–Maastrichtian) from the wells Rigs-1 and Rigs-2 in the northern part of the South Arne Field. These samples are dominated by a kaolinite showing sharp 00*l* peaks in oriented specimens and contain 2:1 layer minerals showing a broad peak at ~12 Å and illite (Figure 3c,d). The kaolinite has a highly ordered structure showing sharp *hkl* reflections (Figure 4). The kaolinite in the residues from several Lower Cretaceous samples in the Valdemar Field to the south of the South Arne Field is structurally similar to the kaolinite from Maastrichtian–Danian chalk in Rigs-1 and Rigs-2, and the residue from Valdemar 2, 2281.4 m is practically pure kaolinite (Table 1b). Therefore, this kaolinite was used as the standard for estimating by XRD the amount of kaolinite in the Maastrichtian–Danian chalk residues from Rigs-1 and Rigs-2, the results for the residues being extrapolated to bulk rock taking into account the amount of calcite removed by dissolution. The kaolinite constituted up to 20% of the chalk, but the amount ranged for most samples from 1% to 5% (Table 1b).

Structural features of mixed-layer clay minerals. For group 1, the XRD patterns of the Mg-saturated samples had, with the exception of one chloritic sample, a very strong peak at 14–15 Å in air-dried and at 17 Å in glycolated specimens and therefore probably corresponded to the smectitic samples reported in many previous investigations. However, modeling of the experimental diffraction effects demonstrated that the

a

Figure 2a detail

b

Figure 2b detail 1

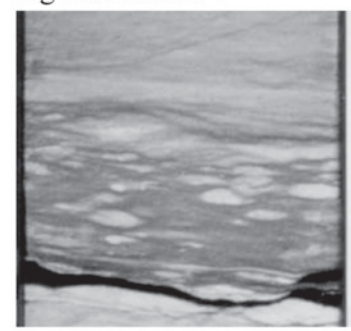

Figure 2b detail 2

samples consisted of two or more mixed-layer phases having S, V, I, and Ch layers (Lindgreen *et al.*, 2002) (Figure 5a,b, Table 2).

In previous studies, for several of the samples, phase compositions and layer sequences obtained by XRD, and structural formulae determined from chemical analysis, IR, ^{27}Al NMR, and Mössbauer spectroscopies, and XRD were published, whereas the octahedral vacancy pattern was obtained by thermal analysis, and particle shape from atomic force microscopy (AFM) (Lindgreen *et al.*, 2002; Drits *et al.*, 2004).

In the present investigation, the samples were divided into six subgroups according to the phases present (Table 3):

Subgroup A consists of one sample, HSI, from the K/T boundary clay-rich layer from Stevns (Tables 2a, 3). This sample is a mixture of HS and LS I-S phases. The HS phase was an almost (0.95) pure smectite, whereas the LS phase contained equal amounts of I and S layers.

Subgroup B includes samples from the gray chalk cropping out at Stevns (sample GRI) and from Danian, Maastrichtian, Santonian, and Campanian chalk, and clay-rich layers from North Sea wells (Tables 2a, 3). These samples consist of a mixture of the HS and LS I-S-Ch phases.

Subgroup C includes two chalk samples from the Santonian and Campanian of well Baron-2 (Tables 2a, 3). These samples contain, in addition to the HS and the LS I-S-Ch phases of subgroup B, a third, mixed-layer (tosudite-like) phase, which had 50% of di-trioctahedral Ch layers alternating regularly with swelling (S or V) dioctahedral layers.

Subgroup D includes Danian and Maastrichtian samples from wells I-1, Q-1 (Q10133R), T-1, and Otto-1 (Tables 2b, 3). These samples contain the HS, the LS I-S-Ch, and the tosudite-like phases of subgroup C. However, a LS I-S-V phase is present in addition to the I-S-Ch.

Subgroup E includes two Danian samples from well I-1, I9106R, and I9149R (Tables 2a, 3), and contains large amounts of a well-crystalline tosudite consisting of regularly alternating Ch and S layers in the ratio 1:1; the

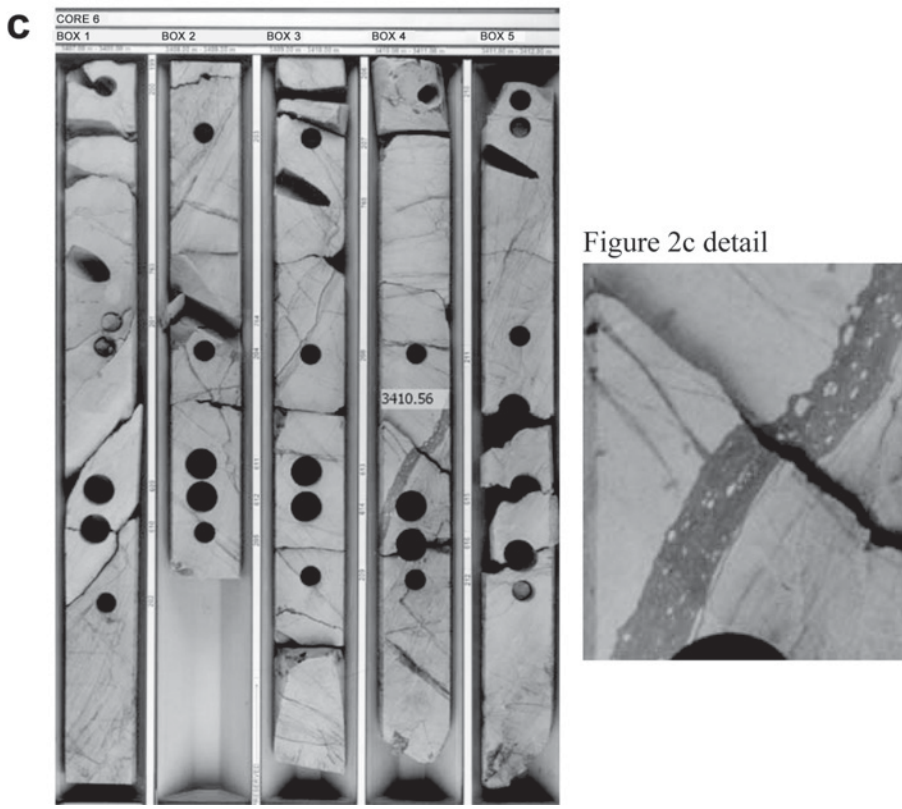

Figure 2 (*facing page and above*). Images of core samples with sample positions listed: (a) Well Rigs-1, Danian, core 2 (box 26–27) and core 3 (box 1–2); positions of clay-layer sample 2822.7 m and of chalk samples at 2823.3 m and 2824.3 m are shown. Detail: 2822.7 m clay layer; shows single seams merging into a composite seam, with chalk lenses. (b) Well Baron-2, core 2 (box 14–18) positions of clay-layer samples (L) and chalk samples (R) are shown. Detail (1): 2859.92 m clay layer: flaser structure with elongate chalk lenses. Detail (2): 2859.09 m clay layer: shows single seams merging into a composite seam. (c) Well SA-1, core 6 (box 1–5), position of the dolomitic seam at 3410.56 m is shown. Detail: 3410.56 m dolomitic seam, showing nodular flaser structure. SA-1 is a deviated well, therefore the core is cut at an angle of 49º.

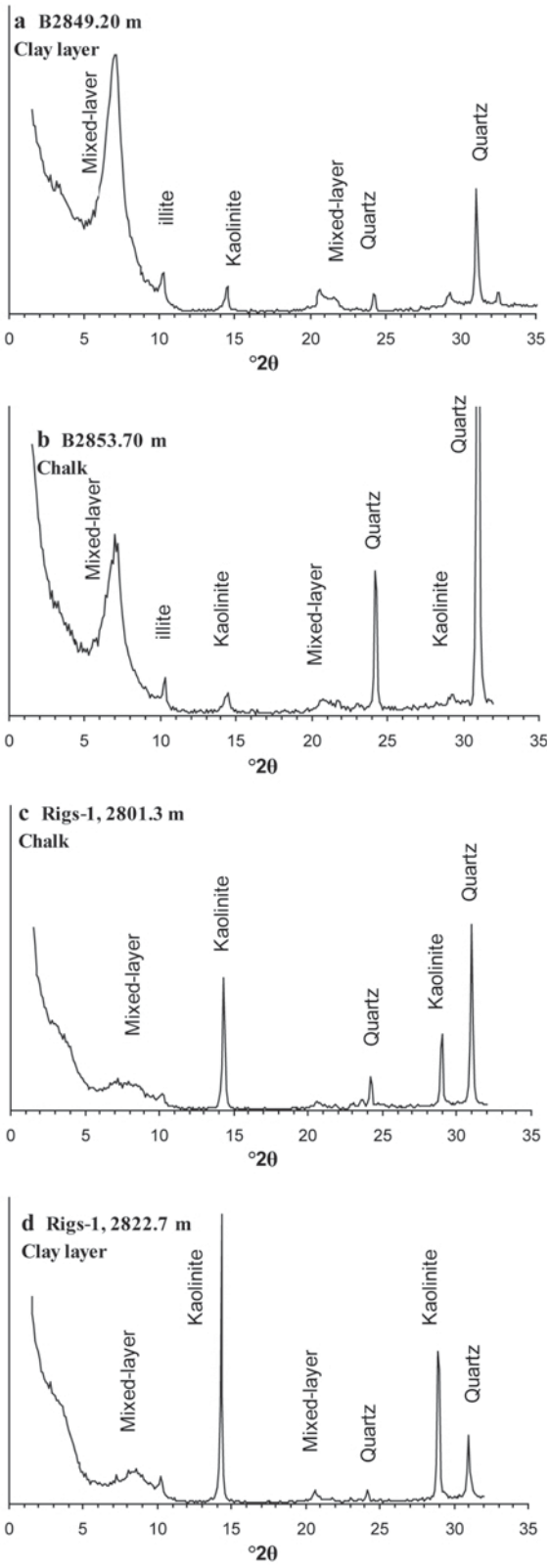

Figure 3. XRD patterns of insoluble residues from the wells Rigs-1 and Baron-2. Oriented specimens, Mg-saturated, air-dried, CoKα radiation.

I-S-Ch is absent. One of the samples, I9106R, has a HS phase and a LS I-S-Ch phase. The second sample, I9149R, has a LS I-S-V phase and the HS phase is absent.

Subgroup F includes a series of Danian samples from chalk in the interval 2860−2867 m of well Baron-2 (Tables 2a, 3). These samples have a LS I-S-V phase and, instead of or in addition to the HS phase, a Ch-Sr phase consisting of 0.90 Ch and 0.10 berthierine layers. In sample B2860R, the HS phase disappeared, and in all samples in the interval 2860−2867m, a phase having 0.70 I layers interstratified with ~0.20 S and ~0.10 V layers formed.

In addition to the mixed-layer phases, most samples contain minor amounts of chlorite and illite.

Evidence for the presence of di-trioctahedral chlorite layers. A methodology (developed by Lindgreen *et al*., 2002) by which the $^{[4]}Al/^{[6]}Al$ ratios determined by ^{27}Al NMR spectroscopy, combined with the results of chemical analysis, allows determination of reliable averaged cation compositions in octahedral and tetrahedral sheets of 2:1 layers and in brucite-like interlayer sheets in a mixture of I-S and I-S-Ch. In the procedure, a coefficient, χ, was calculated from the equation

$$\chi = 4(1 + p)/[(1 + p)C_{SiO_2} + 2pC_{Al_2O_3}]$$

where $p = {}^{[4]}Al/{}^{[6]}Al$ and C_{SiO_2} and $C_{Al_2O_3}$ are the weight percentages of SiO_2 and Al_2O_3 divided by the molecular weights, respectively. For a given p the values χC_{SiO_2}, 2χ Al_2O_3, χ MgO, *etc*. correspond to the number of atoms of Si, Al, Mg, *etc*. in the formula which is based on four tetrahedral cations. If a sample consists of a mixture of I-S and I-S-V differing from each other in their weight concentrations and amounts of the layer types in each phase, then the sum of the octahedral cations, as well as the number of OH groups, should be equal to two. However, if a sample consists of a mixture of I-S and I-S-Ch, then both the amounts of octahedral cations and of (OH) groups should be >2. If the chlorite layers are di-trioctahedral, then they contain five octahedral and four tetrahedral cations per $O_{10}(OH)_8$. The sum of octahedral cations, n, and the number of (OH) groups, m, allow us to calculate the contribution of chlorite layers, x, in the sample studied $x_1 = (n-2)/3$ and $x_2 = (m-2)/6$.

The values of x_1 and x_2 may be slightly different because the samples (except HSI and GRI) contain small amounts of trioctahedral chlorite.

The averaged cation compositions of the tetrahedral and octahedral sheets and of the interlayers of the Na-saturated samples, representing the subgroups of group 1, as well as the corresponding p and x values are shown in Table 4. As expected, for samples HSI (subgroup A) and GRI (subgroup B), which according to XRD data contain no chlorite layers, $m = n = 2.0$ and $x = 0$. In contrast, for the other samples, the amount of

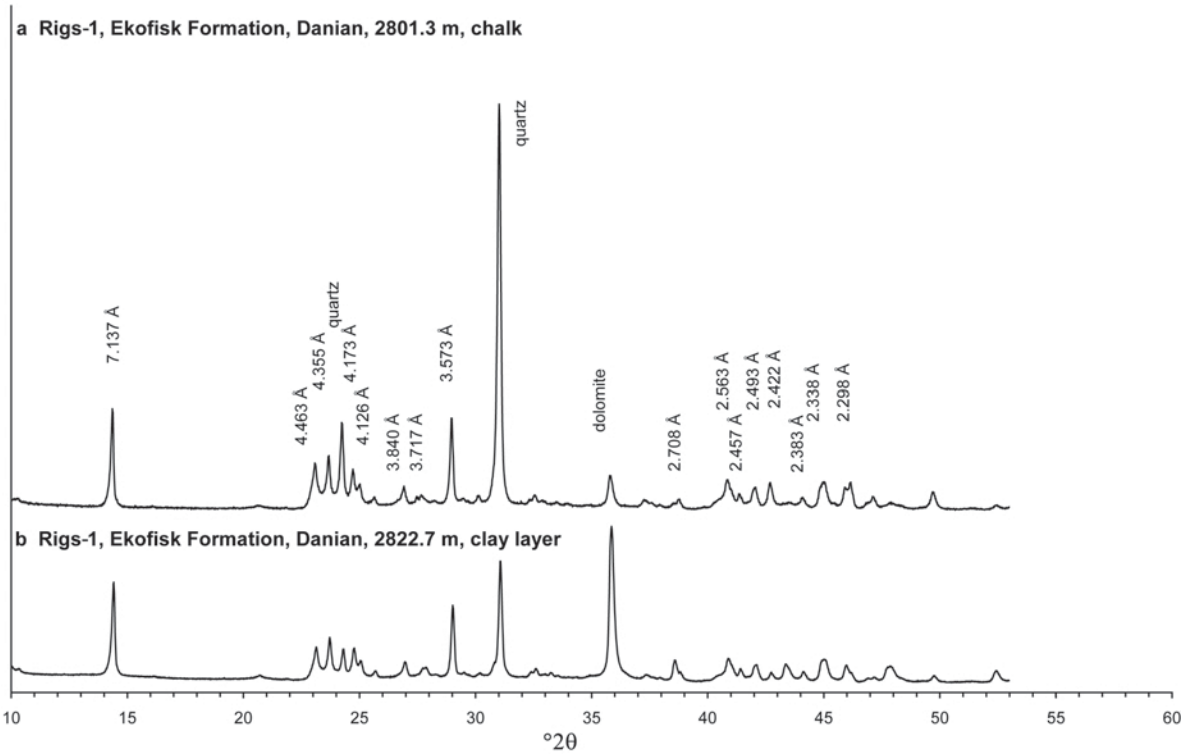

Figure 4. XRD patterns of insoluble residues from the well Rigs-1. Randomly oriented specimens, CoKα radiation.

chlorite layers, as calculated according to the above procedure, varies from 3 to 17%.

The remarkable features of the cation composition of the samples HSI and GRI are the small amount of substitution of Al for Si in the tetrahedral sheets and the large amount of Mg in the octahedral sheets of the 2:1 layers. The cation composition of the tetrahedral and octahedral sheets of the other samples of subgroup B and of samples of subgroups C and D are similar. The structural formula of sample I9149R from subgroup E corresponds to that of tosudite.

Table 4 also contains the amounts of chlorite layers calculated from the results of modeling of the experimental XRD patterns which include the weight concentrations of the coexisting mixed-layer phases and the contents of the layer types in each of them. These data enabled estimation of the amounts of chlorite layers in each sample. For example, sample B 2919L contains 19% of the I-S-Ch and 1% of chlorite where the Ch layers of the I-S-Ch are di-trioctahedral. Because the I-S-Ch contains 0.20 Ch layers, the total number of these layers in this phase is ~4%, and the total amount of chlorite layers is ~5%. Table 4 shows that the two independent techniques confirm the presence of the di-trioctahedral chlorite layers in the studied samples although the amounts of the layers determined by different approaches do not always correlate. The observed discrepancies are associated with: (1) experimental errors in chemical and phase analyses (in determination of structural and probability parameters of the mixed-layer phases) and in $^{[4]}$Al/$^{[6]}$Al ratios; and (2) cation compositions for individual layer types cannot be evaluated accurately from the experimental data available. Therefore, determining the actual molar contents of the layer types precisely in order to provide a careful comparison of the layer content is impossible based on XRD data.

DISCUSSION

Origin of the mixed-layer minerals in the chalk

For group 1 samples, the fact that the octahedral sheets were Mg-rich (Table 4) conformed with an origin from volcanic ash. The similar phase and chemical compositions of a large number of Maastrichtian samples of subgroup B (*e.g.* from outcrop GRI at Stevns and from the Mona well in the Central Trough at 3200 m depth) indicate that a single parent material composition was present over most of the Maastrichtian basin, and the similar phase composition of Danian and Maastrichtian samples suggest a single parent material composition during Maastrichtian–Danian time (Lindgreen *et al.*, 2002). Drits *et al*. (2004) concluded that the I-S minerals in the Stevns clay-rich layer sample HSI of subgroup A had formed from volcanic ash, and, furthermore, that the mixed-layer minerals in the other

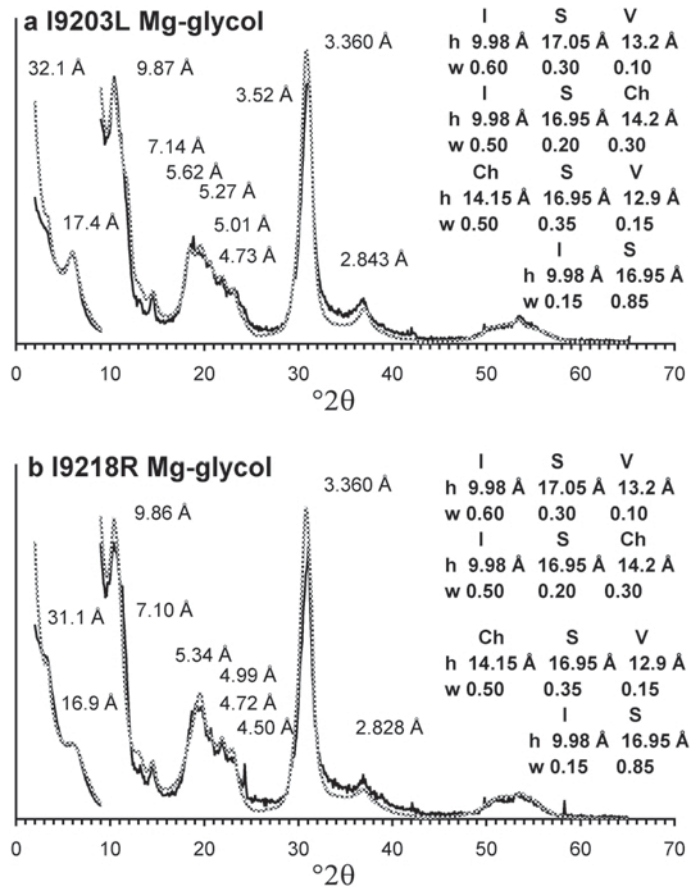

Figure 5. Experimental (jagged) and simulated (smooth) XRD patterns for samples dominated by mixed layers from well I-1. Oriented specimens, Mg-saturated and glycolated. For each phase, the content (w) and thickness (h) of the interstratified layers are shown, together with the experimental *d* values. The scale above 9º2θ has been increased 20 times in order to demonstrate the agreement between experimental and calculated patterns. CoKα radiation. The minor differences between the patterns for the two samples are due to minor differences in the proportions of the phases (see Table 2b).

samples of group 1 had formed by diagenesis of I-S minerals such as those of the HSI sample. This diagenesis took place through replacement of smectite interlayers by $(MgAl)(OH)_2$ sheets and the formation of di-trioctahedral layers in the LS phase, together with illitization through an increase in tetrahedral charge and fixation of K in the HS phase to form mixtures of I-S-Ch and I-S (subgroup B). Further diagenesis at a higher temperature formed tosudite-like, ordered Ch-S (subgroups C, D, and E) and Ch-Sr (subgroup F) (Lindgreen *et al*., 2002).

The mixed-layer minerals of subgroup B prevailed in well Baron-2, but within this group, small differences in proportion of the phases were notable in this and in other wells. One example is that B2853R (2853.7 m) and B2855L (2855.3 m) have identical proportions of the phases, whereas B2849L (2849.2 m) has a smaller HS content and a greater I-S-Ch content. A second example is that B2885L (2885.3 m) and B2886R (2886.8 m) are identical, whereas B2873R (2873.1 m) has a smaller HS content and a larger I-S-Ch content (Table 2a). These differences may be assigned to small differences in the amounts of di-trioctahedral chlorite layers formed during diagenetic transformation of the low smectite I-S into the I-S-Ch prior to the formation of the clay-rich layers. However, the occurrence in well Baron-2 of the subgroup D mixed-layer minerals in one Campanian and one Santonian chalk sample shows that local heating has taken place, as tosudite-like minerals typically form at ~100ºC in hydrothermal systems (Inoue and Utada, 1991). The finding of only the strongly transformed mixed-layer minerals of the subgroups D and E in well I-1 might be related to the fact that the well was drilled on the crest of the structure and the crest is strongly intersected by faults, which may have facilitated the migration of fluids from deeper layers. Furthermore, the strongly transformed minerals of subgroup F from well Baron-2, 2860−2867 m, are present in the interval between two clay-rich layers at 2859.99 m and 2866.83 m in Baron-2 and may have formed after the formation of the seams, possibly due to migration of fluids in the chalk.

Origin of the kaolinite in wells Rigs-1 and Rigs-2

The kaolinite seen by Maliva *et al*. (1999) in the chalk of the Eldfisk, Tor, and Machar fields was disordered and thus different from the 3D ordered kaolinite of the Rigs-1 and Rigs-2 wells. Maliva *et al*. (1999) concluded that the Eldfisk, Tor, and Machar field kaolinites formed diagenetically from organic-rich pore fluids in the chalk. However, in the South Arne Field, such a process would be expected to take place not only in Rigs-1 and Rigs-2, where the kaolinite was found, but also in the I-1 and SA-1 wells, which are oil-bearing wells like Rigs-1 and Rigs-2, but where the dominant clay minerals in fact are the mixed layers of group 1. The hypothesis of Maliva *et al*. (1999) therefore cannot explain the occurrence of kaolinite in Rigs-1 and Rigs-2.

In the South Arne Field, the local occurrence of the 3D ordered kaolinite in the Maastrichtian–Danian chalk was restricted to the wells Rigs-1 and Rigs-2. The insignificant amount of kaolinite in the corresponding chalk sections of SA-1, I-1, and Baron-2 in the same field and in the other wells in the adjacent area rules out the deposition of kaolinite of detrital origin on a regional scale, but indicates a local origin of the kaolinite in Rigs-1 and Rigs-2. The northern part of the South Arne Field is characterized by thin Maastrichtian chalk directly overlying truncated Lower Cretaceous sediments, because the crestal part of the structure was elevated here to a depth where severe sub-marine erosion of the Lower Cretaceous deposits took place during Campanian and early Maastrichtian. Albian Shale and Upper Sola chalk are absent from Rigs-1 and Rigs-2. To the south, the wells I-1 and Baron-2 consist of a nearly complete Lower Cretaceous succession overlain by the Upper Cretaceous Hod Formation. The same sequence was seen in the Valdemar field.

Unfortunately, core material from Lower Cretaceous is not available from the northern part of the South Arne structure. However, in the Valdemar Field to the south of the South Arne Field, several cores have been taken in Lower Cretaceous formations. In these cores, the lower part of Lower Cretaceous – the Valhall, Tuxen, and Lower Sola Formations – contained kaolinite together with smectitic clay minerals (Jakobsen *et al*., 2002). However, for the youngest Lower Cretaceous, the Upper Sola, Albian Shale, and Rødby formations, the dominant clay mineral was a 3D-ordered kaolinite similar to that found in Maastrichtian–Danian chalk and clay layers in Rigs-1 and Rigs-2. During deposition of the Maastrichtian and Danian chalk in Rigs-1 and Rigs-2, reworked Lower Cretaceous sediments might therefore have been incorporated into the overlying formations.

Formation of seams and clay-rich layers

Comparison with adjacent chalk. In the case of well SA-1 containing significant amounts of dolomite in the Maastrichtian samples, the dolomites in the solution seam at 3410.6 m and in the chalk sample taken immediately above (3410.6 m) were practically identical. The residues of both samples contained the same blocky, pitted crystals of dolomite (Figure 6a,b). The identical thermal evolution of CO_2 curves over the 700–900ºC range, where carbonates release CO_2 (Figure 7a,b), demonstrate, together with the identical powder XRD patterns, that the dolomite has the same layer structure and chemical composition in the two residues.

The clay mineralogy was also similar for the seams or clay-rich layers and the adjacent chalk. This was very clear when comparing the two wells Rigs-1 and Rigs-2 (Figure 4) which have large amounts of kaolinite in the clay layers and in the chalk, with all other wells investigated in the area having mainly illite-smectite mixed-layer minerals in the clay layers and in the chalk (Figures 3, 4).

Furthermore, the detailed structural characterization and subgrouping of the samples dominated by mixed layers (Tables 2, 3) revealed that in most cases their structures were similar for the seams and for the adjacent chalk. For example, the samples from an 8 m thick

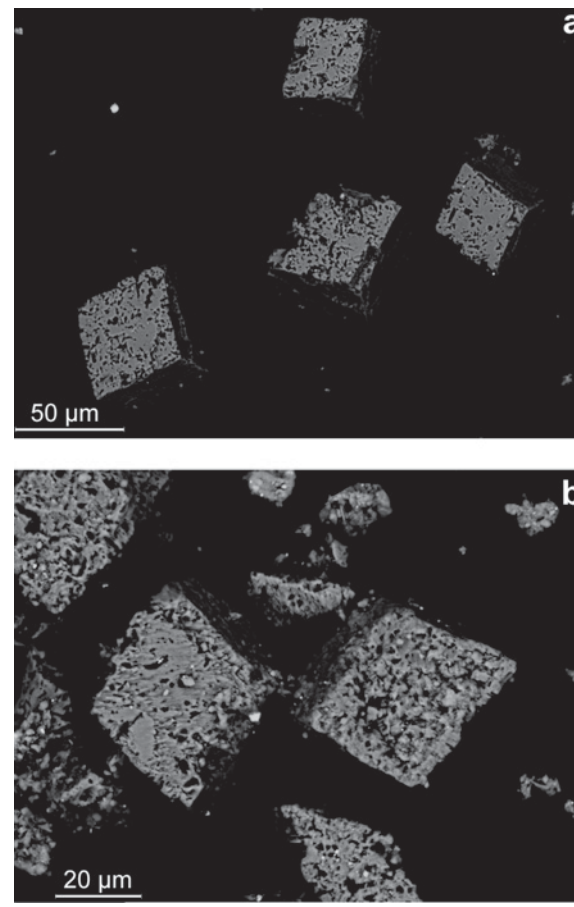

Figure 6. SEM images of the insoluble residues from the well SA-1, the chalk adjacent to the seam (a) and the seam (b).

Table 2a. Structural and probability parameters for the HS and LS phases and phase composition (weight content) of subgroup A, B, C, E, and F samples determined by XRD.

Sample	HS phase					LS phase							Amounts of phases				
	h_S	h_V	w_S	w_V	N	h_S	h_V	h_{Ch}	w_S	w_V	w_{Ch}	N	HS	LS	I	Ch	T
Subgroup A																	
HSI	16.76		0.95		4.5	16.76			0.50			4.0	70	30	–	–	–
Subgroup B																	
L9445R	16.95	12.9	0.75	0.10	4.5	16.95		14.2	0.30		0.20	5.5	46	44	7	3	–
M10446R	16.85	12.9	0.75	0.10	3.5	16.95		14.2	0.30		0.20	5.5	66	29	5	–	–
M10448R	16.95	12.9	0.75	0.10	3.5	16.95		14.2	0.30		0.20	5.5	76	17	5	1	–
M10470R	16.85	12.9	0.75	0.10	3.5	16.95		14.2	0.30		0.20	5.5	45	48	7	–	–
GRI	16.85	12.9	0.75	0.10	4.5	16.95		14.2	0.30		0.20	5.5	73	20	7	–	–
B2849L	17.05	12.9	0.75	0.10	4.5	16.95		14.2	0.30		0.20	5.5	61	30	7	2	–
B2853R	17.05	12.9	0.75	0.10	4.5	16.95		14.2	0.30		0.20	5.5	70	20	7	3	–
B2855L	17.05	12.9	0.75	0.10	4.5	16.95		14.2	0.30		0.20	5.5	70	20	7	3	–
B2870L	16.95	12.9	0.75	0.10	4.5	16.85		14.2	0.30		0.20	5.5	47	40	8	5	–
B2872L	16.95		0.85		3.5	16.85		14.2	0.30		0.20	5.5	44	44	9	3	–
B2873R	16.95		0.85		3.5	16.85		14.2	0.30		0.20	5.5	55	35	6	4	–
B2885L	16.85		0.85		5.5	16.95		14.2	0.30		0.20	5.5	73	21	5	1	–
B2886R	16.85		0.85		5.5	16.95		14.2	0.30		0.20	5.5	73	21	5	1	–
B2895L	16.85	12.9	0.65	0.10	5.5	16.95		14.2	0.30		0.20	5.5	70	20	9	1	–
B2895R	16.85		0.85		5.5	16.95		14.2	0.30		0.20	5.5	58	36	5	1	–
B2900R	16.85		0.85		5.5	16.95		14.2	0.30		0.20	5.5	73	21	5	1	–
B2908L	16.80		0.55		6.5	16.70		14.1	0.30		0.20	5.5	64	20	15	1	–
B2919L	16.85		0.85		5.5	16.95		14.2	0.30		0.20	5.5	79	19	2	1	–
T7349R	Structure and phase composition similar to T7398R (not simulated in detail).																
T7398R	16.80		0.90		5.5	16.95		14.2	0.30		0.20	5.5	72	20	7	1	–
T7618L	16.70	12.9	0.80	0.05	4.5	16.95		14.2	0.30		0.20	5.5	50	33	14	3	–
T7621L	16.75		0.75		4.5	16.95		14.2	0.30		0.20	5.6	54	40	5	1	–
O8117R	16.95		0.85		6.0	16.95		14.2	0.30		0.15	6.0	70	24	5	1	–
O8135R	16.85		0.85		6.0	16.95		14.2	0.30		0.15	6.0	64	30	5	1	–
Subgroup C																	
B2876R	16.85		0.85		5.5	16.85		14.2	0.30		0.20	5.5	52	38	–	3	7
B2926R	16.80		0.85		5.0	16.95		14.2	0.30		0.20	5.5	53	27	1	1	18
Subgroup E																	
I9106R	16.6		0.65		4.5	17.05	13.2		0.30	0.10		7.0	62	9	3	5	21
I9149R						16.9	13.5		0.20	0.25		7.0	–	67	–	–	33
Subgroup F																	
B2860R	*					16.85	13.2		0.20	0.10		8.0	0*	40	7	–	–
B2863aR	$^{+}$16.60	12.9	0.90	0.10	3.8	16.86	12.9		0.25	0.05		8.0	52^{+}	42	–	–	–
B2863bR	$^{+}$16.60	12.9	0.90	0.10	3.8	16.86	12.9		0.25	0.05		8.0	52^{+}	42	–	–	–
B2867R	$^{\wedge}$16.90	12.9	0.60	0.10	4.5	16.85	13.2		0.20	0.05		8.0	$41^{\wedge}$	21	3	–	–

* contains 53% of a chlorite-serpentine phase consisting of 14.19 Å (0.90) chlorite and 7.20 Å (0.10) berthierine and with N = 10 instead of the HS phase.
+ contains 6% of a chlorite-serpentine phase consisting of 14.12 Å (0.90) chlorite and 7.06 Å (0.10) berthierine and with N = 8
^ contains 36% of a chlorite-serpentine phase consisting of 14.12 Å (0.90) chlorite and 7.06 Å (0.10) berthierine and with N = 8
h_S, h_V, and h_{Ch}: thicknesses of smectite, vermiculite, and chlorite layers, respectively.
w_S, w_V, and w_{Ch}: proportions of smectite, vermiculite, and chlorite layers, respectively.
N: mean number of layers in the CSDs.

Table 2b. Structural and probability parameters for the HS and LS phases and phase composition (weight content) of subgroup D samples determined by XRD.

Sample	Phase	h_S	w_S	N	Phase	h_S	h_V	h_{Ch}	w_S	w_V	w_{Ch}	N	Amounts of phases					
													HS	LS_{I-S-V}	LS_{I-S-Ch}	T	I	Ch
I9192R					LS_{I-S-V}	17.05	13.2		0.30	0.10		7.0	0	74.5	9	9	4.5	3
					LS_{I-S-Ch}	16.95		14.20	0.20		0.30	5.5						
					T	16.95	12.9	14.15	0.35	0.15	0.50	8.0						
I9203L	HS	16.95	0.85	4.5	LS_{I-S-V}	17.05	13.2		0.30	0.10		7.0	14	50	14	17	4	1
					LS_{I-S-Ch}	16.95		14.20	0.20		0.30	5.5						
					T	16.95	12.9	14.15	0.35	0.15	0.50	8.0						
I9218R	HS	16.95	0.85	3.5	LS_{I-S-V}	17.05	13.2		0.30	0.10		7.0	5	61	10	20	3	1
					LS_{I-S-Ch}	16.95		14.20	0.20		0.30	5.5						
					T	16.95	12.9	14.15	0.35	0.15	0.50	8.0						
Q10133R	HS	16.95	0.80	4.5	LS_{I-S-V}	16.85	13.2		0.30	0.10		7.5	14	17	28	30	3	8
					LS_{I-S-Ch}	16.95		14.20	0.30		0.20	5.5						
					T	16.95	12.9	14.15	0.35	0.15	0.50	8.0						
T7269R	HS	16.85	0.80	4.5	LS_{I-S-V}	16.85	13.2		0.30	0.10		7.0	32	23	28	0	6	0
					LS_{I-S-Ch}	16.95		14.20	0.30		0.20	5.5						
T7491R	HS	16.65	0.67	4.5	LS_{I-S-V}	16.75	12.9		0.30	0.10		7.0	67	10	0	20	1	2
					T	16.95	12.9	14.15	0.35	0.15	0.50	8.0						
T7512R	HS	16.60	0.80	4.5	LS_{I-S-V}	16.75	12.9		0.30	0.10		7.0	27	10	40	20	1	2
					LS_{I-S-Ch}	16.65		14.20	0.40		0.10	5.5						
					T	16.95	12.9	14.15	0.35	0.15	0.50	8.0						
O8152R	HS	16.75	0.80	4.5	LS_{I-S-V}	16.75	12.9		0.30	0.10		7.0	19	35	25	17	1	3
					LS_{I-S-Ch}	16.95		14.20	0.30		0.20	5.5						
					T	16.95	12.9	14.15	0.35	0.15	0.50	8.0						

Legend: see Table 2a.

Table 3. Group 1 mixed-layer mineral samples divided into subgroups. Occurrence and phases present.

Sub-group	Samples	Strat.	Depth	Phases present						
				HS	LS_{I-S}	LS_{I-S-V}	LS_{I-S-Ch}	Ch-Br	T	Others
A	HSI	Dan/Maas	Outcrop	x	x					
B	GRI	Maas	Outcrop	x			x			I, (Ch)
	L9445R, B2849L, B2853L, B2853R, B2855L, B2870L, B2872L, B2873R, B2885R, T7349R, T7398R, O8117R, O8135R M10446R, M10448R, M10470R, T7618L, T7621L B2886R, B2895L, B2895R, B2900R, B2908L, B2919L	Danian	2239–2885 m							
		Maas	2320–3192 m							
		Sant.–Camp.	2886–2919 m							
C	B2876R, B2926R	Sant.–Camp.	2876–2926 m	x			x		x	(I), Ch
D	T7269R, O8152R(D/M)	Danian	2215–2485 m	x		x	x		(x)	I, (Ch)
	I9192R, I9203L, I9218R, T7491R, T7512R	Maas.	2283–2810 m	(x)		(x)	(x)		x	I, Ch
E	I9106R, I9149R	Danian	2775–2789 m	(x)		x			x	(I, Ch)
F	B2860R, B2863aR, B2863bR, B2867R	Danian	2860–2867 m	(x)		(x)		x		(I)

( ) indicates that the phase is present in some samples.

interval of Maastrichtian chalk in well I-1: the chalk sample I9192R (2801.7 m), the clay layer sample I9203L (2805.1 m), and the chalk sample I9218R (2809.6 m) are all of the same diagenetically transformed subgroup D (Figure 5a,b). Small differences in proportions of the phases (Table 2b) might, as argued above, be assigned to differences in the original mixed-layer minerals in the chalk. Similarly, the identical composition of the mixed-layer minerals of clay-rich layers and the chalk was seen for the clay-rich layer sample B2855L (2855.3 m) and the adjacent chalk sample B2853R (2853.7 m) and between the clay-rich layer sample B2885L (2885.3 m) and the adjacent chalk B2886R (2886.8 m) (Table 2a).

Models for formation

Concentrated ash falls. As described above, the mixed-layer minerals probably originated from volcanic ash sedimented simultaneously with chalk sedimentation and constituted a small fraction of the chalk. The clay-rich layers have been attributed to periods of deposition of predominantly volcanic ash (Wray, 1995, 1999; Simonsen and Toft, 2006). However, this hypothesis is

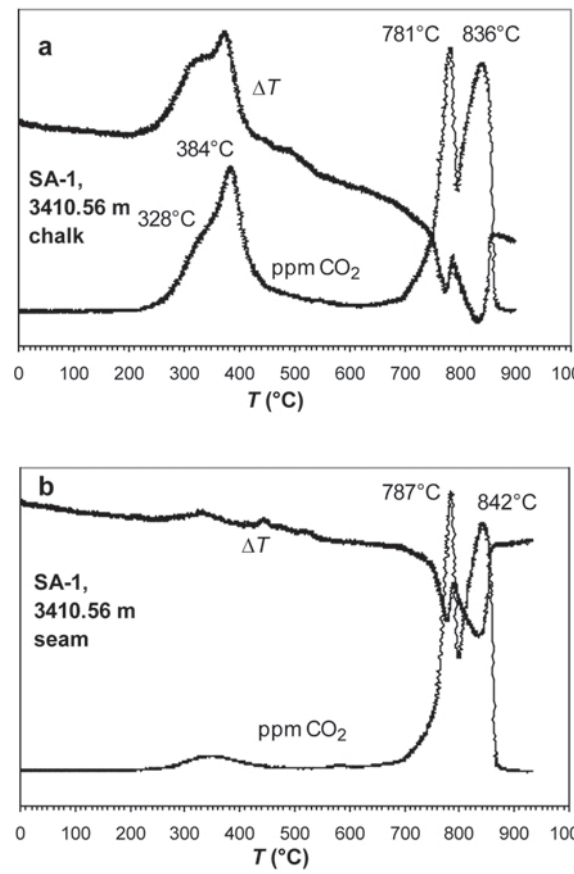

Figure 7. Thermal analysis (DTA-CO_2 evolution) of insoluble residues from well SA-1, the chalk adjacent to the seam (a) and the seam (b); heating at 10ºC/min, flow of 400 mL/min of 40% O_2 in N_2.

Table 4. Average cation composition of tetrahedral and octahedral sheets and interlayers in the Na-saturated samples studied. Evidence is seen for the presence of ditrioctahedral chlorite layers in the structures of the samples.

Sample	Si	$^{[4]}$Al	$^{[6]}$Al	Fe	Mg	*n*	K	Na	$^{[4]}$Al/$^{[6]}$Al[1]	$O_{10}(OH)_m$[2]	% of chlorite layers (x) From NMR	From XRD
Subgroup A												
HSI	3.94	0.06	1.30	0.16	0.54	2.00	0.07	0.44	0.048	$O_{10}(OH)_2$	0	0
Subgroup B												
GRI[3]	3.91	0.09	1.19	0.25	0.56	2.00	0.09	0.12	0.072	$O_{10}(OH)_2$	0	0
B2855L	3.80	0.20	1.56	0.17	0.36	2.09	0.17	0.20	0.13	$O_{10}(OH)_{2.08}$	2	7
B2870L	3.76	0.24	1.59	0.22	0.49	2.30	0.23	0.20	0.15	$O_{10}(OH)_{2.60}$	10	13
B2872L	3.80	0.20	1.64	0.19	0.47	2.30	0.24	0.13	0.12	$O_{10}(OH)_{2.60}$	10	12
B2876R	3.83	0.17	1.68	0.18*	0.53	2.39	0.18	0.20	0.10	$O_{10}(OH)_{2.78}$	13	10
B2885L	3.82	0.18	1.61	0.12	0.46	2.19	0.16	0.36	0.11	$O_{10}(OH)_{2.45}$	6	5
B2895L	3.84	0.16	1.62	0.14**	0.50	2.26	0.29	0.20	0.12	$O_{10}(OH)_{2.58}$	9	5
B2895R	3.84	0.16	1.62	0.12	0.50	2.24	0.17	0.32	0.10	$O_{10}(OH)_{2.55}$	9	8
B2919L	3.84	0.16	1.57	0.12	0.43	2.12	0.17	0.26	0.10	$O_{10}(OH)_{2.21}$	4	6
Subgroup C												
B2926R	3.83	0.17	1.71	0.14	0.55	2.40	0.14	0.25	0.10	$O_{10}(OH)_{2.87}$	14	15
Subgroup D												
I9203L	3.76	0.24	1.63	0.13	0.42	2.18	0.29	0.20	0.15	$O_{10}(OH)_{2.37}$	6	13
I9218R	3.75	0.25	1.55	0.15	0.46	2.16	0.27	0.25	0.16	$O_{10}(OH)_{2.30}$	5	14
Subgroup E												
I9149R	3.66	0.34	1.69	0.23***	0.58	2.50	0.26	0.23	0.20	$O_{10}(OH)_{3.00}$	17	17

[1]: Al-MAS NMR; [2]: average anion composition; [3]: Ca-saturated
*: Fe^{3+} and Fe^{2+}: 0.10 and 0.07
**: Fe^{3+} and Fe^{2+}: 0.10 and 0.04
***: Fe^{3+} and Fe^{2+}: 0.16 and 0.07

invalid for the region of the North Sea including the South Arne Field. First, because the I-S rich layers were absent in the Maastrichtian–Danian chalk of wells Rigs-1 and Rigs-2, and because the kaolinite present in large amounts in all Maastrichtian–Danian clay-rich layers from Rigs-1 and Rigs-2 cannot form from volcanic ash in a high-ionic environment or at the neutral to alkaline conditions in the chalk (Millot, 1970). Second, because of the find of identical phase compositions and structure of the fine clays in the chalk and the adjacent clay-rich layers.

Dissolution of calcite. The merging of thin seams into larger seams as described by Safaricz and Davison (2005) was observed, *e.g.* in Baron-2 at 2866.8 m and at 2859.92 m (Figure 2b). The seam at 2859.92 m, with chalk lenses, closely resembles the flaser structures described by Garrison and Kennedy (1977, their fig. 10). Most of the seams in the chalk were parallel to bedding, as described by Davison *et al.* (2000), but some were inclined. Solution seams and flaser structures have been proposed to originate from two main processes: (1) dissolution-reprecipitation during early diagenesis; or (2) the differential responses to stress of interlayered competent and incompetent sediment occurring rather late in burial diagenesis (Garrison and Kennedy, 1977). D'Heur (1984) described the pressure-solution process as part of the chemical compaction taking place in the water zone of chalk reservoirs, whereas this process did not take place in the oil zone, which then remained highly permeable. For Upper Cretaceous chalk of southern England, Garrison and Kennedy (1977) concluded that the seams and flaser structures formed during late burial diagenesis due to mechanical compaction and pressure solution of calcium carbonate. Furthermore, the dissolution was most intense in the originally most argillaceous parts of the chalk. Generally, pressure solution has been the favored mechanism for formation of the seams and flaser structures (*e.g.* D'Heur, 1984; Egeberg and Saigal, 1991; Mallon and Swarbrick, 2002; Safaricz and Davison, 2005). The finding in SA-1, at 3410.56 m, that the dolomite crystals were similar in shape and composition to those of the adjacent chalk demonstrated that the formation of the seam resulted from the sole solution of calcite and not dolomite. Similarly, the identical structures of the mixed-layer minerals in the clay-rich layers and in adjacent chalk demonstrated that the clay minerals had also not been affected. That only calcite had been dissolved indicates strongly that the clay layers and seams did not form by pressure solution, but simply by dissolution of the calcite and removal of the ions by fluids migrating in the chalk followed by compaction. From the thickness of the seam (1.5 cm) and the proportion of dolomite in the seam and

the adjacent chalk (Table 1a), one can calculate that the seam at 3410.6 m in well SA-1 formed from dissolution of ~15 cm of chalk. The formation of dolomite in North Sea chalk was shown by Maliva and Dickson (1994) to be a late diagenetic event, taking place at burial depths of >1 km, and the dolomitic seam in SA-1 must have formed later than such a late diagenetic dolomite formation. In the North Sea chalk reservoirs, Garrison and Kennedy (1977) estimated the formation of flaser structures and chemical compaction to take place at burial depths of 0.3−2 km, and Taylor and Lapré (1987) estimated chemical compaction to be initiated at 0.8−1 km depth, simultaneously with or shortly after oil filling the reservoir. The fact that the mixed-layer minerals in the clay-rich layers had the subgroup B I-S-Ch phase and not the LS phase as in subgroup A sample HSI showed that the mixed-layer minerals in the clay-rich layers had been diagenetically transformed in chalk by the interlayering of $(MgAl)(OH)_2$ between smectite layers before dissolution of the calcite. Similarly, the dolomite formed in the chalk of SA-1 through Mg-supply before the dissolution of the chalk at 3410.56 m and the formation of the dolomite seam took place.

Morse and Mackenzie (1990) concluded that even small variations in subsurface fluid composition (*e.g.* salinity) could cause much greater changes in solubility of carbonate phases compared to the effect from increasing pressure and temperature associated with sediment burial. Furthermore, a decrease in pH of the pore fluid should result in strongly increased solubility of calcite. Safaricz and Davison (2005) concluded that the Cretaceous–Paleocene chalk from the North Sea was, in fact, an open pressure-solution system due to the large fluid volume involved in the chalk dissolution. Migration of water solutions in the chalk reservoirs was advocated and discussed by D'Heur (1984), Rabinowicz *et al.* (1985), Egeberg and Aagaard (1989), Jensenius (1987), and Mallon and Swarbrick (2002). However, Egeberg and Saigal (1991) concluded from petrographic and chemical (elements and isotopes) studies that fracture-filling calcite probably formed in a closed system. Removal of the calcite corresponding to 15 cm of chalk dissolved in the 3410.6 m seam in SA-1 and the calcite removed during formation of the clay-rich layers must, however, implicate an open system. The fluids must have had a pH sufficient to dissolve calcite but not the dolomite. The release of Mg from dolomite is slow compared to the release of Ca (Pokrovsky and Schott, 2002; Gaultier *et al.*, 2007; Zhang *et al.*, 2007), and the dissolution of dolomite displays a half-order dependence on the crystal/solution interfacial concentration of H^+ compared to the first-order dependence of calcite (Orton and Unwin, 1993). The migrating fluids must, at the same time, have contained an amount of cations such that the I-S-Ch and HS phases of the samples dominated by mixed layers were not changed. Formation waters from some Norwegian North Sea chalk reservoirs in the Ekofisk Field had a pH of 6.0−6.5 (Egeberg and Aagaard, 1991) and the concentration of HCO_3^- was <700 mg/L (Warren *et al.*, 1994). The pK_a values for H_2CO_3 in seawater are 5.8 and 8.9 (Prieto and Millero, 2002). Therefore, the ion of this acid in the formation waters was HCO_3^-, and the dissolution of calcite took place until the concentration of Ca^{2+} had increased sufficiently to exceed the solubility product for $CaCO_3$. At this stage some disordered biogenic calcite dissolved, and pure, ordered, inorganic calcite precipitated as calcite cement due to the entropy effect. However, dissolution of the calcite and formation of the seams and clay-rich layers require a flow of water solutions through the seams and clay layers as also suggested by Safaricz and Davison (2005), in order to remove Ca^{2+}. In conclusion, the dissolution of calcite and the formation of the clay layers and seams were probably due to migration of water solutions through permeable layers in the chalk.

CONCLUSIONS

For the Upper Cretaceous−Danian chalk of the North Sea, mixed layers were the dominant clay minerals, except for two wells, Rigs-1 and Rigs-2, in which a kaolinite with a 3D-ordered structure prevailed. For the samples dominated by mixed-layers, two illite-smectite phases, a high-smectite (HS) one and a low-smectite illite-smectite-chlorite (I-S-Ch) one, prevailed in most of the samples irrespective of depth or location of the samples. However, some samples contained phases of I-S-Ch and ordered S-Ch, and others a chlorite-serpentine (Ch-Sr) phase, and these samples probably formed during diagenesis at higher temperatures. The clay-rich layers and the adjacent chalk had the same clay mineralogy, both with respect to type of clay mineral (kaolinite *vs*. mixed-layer minerals) and with respect to structure of the mixed-layer varieties. One seam investigated contained dolomite having a structure identical to the structure of the dolomite in the adjacent chalk. The identical or very similar phase compositions of the fine clays in the chalk and the adjacent clay-rich layers; the presence of large amounts of kaolinite in the clay-rich layers; and, simultaneously, the absence of clay-rich layers dominated by mixed-layer minerals in the Maastrichtian−Danian section of the two wells Rigs-1 and Rigs-2; as well as the identical chemical composition and particle morphology of dolomites in a seam of well SA-1, demonstrated that the clay-rich layers and seams formed as a result of the dissolution of the calcite matrix, but not from sedimentation and transformation of volcanic ash. The layers probably formed due to migration of water solutions through permeable layers in the chalk. The pH of the migrating solutions is suggested to be the main factor in the dissolution process.

ACKNOWLEDGMENTS

The authors thank N. Springer for discussions on sampling and pore-water chemistry. V.A. Drits and B.A. Sakharov thank the Russian Foundation for Fundamental Investigation (RFFI) for partial financial support. The authors are grateful to B. Lanson, A. Meunier, and J. Cuadros for constructive reviews.

REFERENCES

Davison, I., Alsop, G.I., Evans, N.G., and Safaricz, M. (2000) Overburden deformation patterns and mechanisms of salt diapir penetration in the Central Graben, North Sea. *Marine and Petroleum Geology*, **17**, 601–618.

Deconinck, J.F. and Chamley, H. (1995) Diversity of smectite origins in Late Cretaceous sediments: Example of chalks from Northern France. *Clay Minerals*, **30**, 365–379.

Deconinck, J.-F., Amédro, F., Baudin, F., Godet, A., Pellenard, P., Robaszynski, F., and Zimmerlin, I. (2005) Late Cretaceous palaeoenvironments expressed by the clay mineralogy of Cenomanian-Campanian chalks from the east of the Paris Basin. *Cretaceous Research*, **26**, 171–179.

D'Heur, M. (1984) Porosity and hydrocarbon distribution in the North Sea chalk reservoirs. *Marine and Petroleum Geology*, **1**, 211–238.

Drits, V.A. and Sakharov, B.A. (1976) *X-ray Analysis of Mixed-layer Minerals*. Nauka, Moscow, 256 pp. (in Russian).

Drits, V.A., Weber, F., Salyn, A.L., and Tsipursky, S.L. (1993) X-ray identification of one-layer illite varieties: Application to the study of illites around uranium deposits of Canada. *Clays and Clay Minerals*, **41**, 389–398.

Drits, V.A., Środoń, J., and Eberl, D.D. (1997) XRD measurements of mean crystallite thickness of illite and illite/smectite: Reappraisal of the Kübler index and the Scherrer equation. *Clays and Clay Minerals*, **45**, 461–475.

Drits, V.A., Lindgreen, H., Sakharov, B.A., Jakobsen, H.J., and Zviagina, B.B. (2004) The detailed structure and origin of clay minerals at the Cretaceous/Tertiary boundary, Stevns Klint (Denmark). *Clay Minerals*, **39**, 367–390.

Egeberg, P.K. and Aagaard, P. (1989) Origin and evolution of formation waters from oil fields on the Norwegian shelf. *Applied Geochemistry*, **4**, 131–142.

Egeberg, P.K. and Saigal, G.C. (1991) North Sea chalk diagenesis: cementation of chalks and healing of fractures. *Chemical Geology*, **92**, 339–354.

Garrison, R.E. and Kennedy, W.J. (1977) Origin of solution seams and flaser structure in Upper Cretaceous chalks of Southern England. *Sedimentary Geology*, **19**, 107–137.

Gaultier, M., Schott, J., and Oelkers, E.H. (2007) An experimental study of dolomite dissolution rates at 80ºC as a function of chemical affinity and solution chemistry. *Chemical Geology*, **242**, 509–517.

Hansen, P.L. and Lindgreen, H. (1989) Mixed-layer illite/smectite diagenesis in Upper Jurassic claystones from the North Sea and onshore Denmark. *Clay Minerals*, **24**, 197–213.

Inoue, A. and Utada, M. (1991) Smectite to chlorite transformation in thermally metamorphosed volcanoclastic rocks in the Kamikata area, northern Honshu, Japan. *American Mineralogist*, **76**, 628–640.

Jakobsen, F., Lindgreen, H., and Springer, N. (2000) Precipitation and flocculation of spherical nano-silica in North Sea chalk. *Clay Minerals*, 35, 175–184.

Jeans, C.V. (1968) The origin of the montmorillonite of the European chalk with special reference to the Lower Chalk of England. *Clay Minerals*, **7**, 311–329.

Jeans, C.V. (2006) Clay mineralogy of the Cretaceous strata of the British Isles. *Clay Minerals*, **41**, 47–150.

Jeans, C.V., Merriman, J., Mitchell, J.G., and Bland, D.J. (1982) Volcanic clays in the Cretaceous of southern England and northern Ireland. *Clay Minerals*, **17**, 105–156.

Jensenius, J. (1987) High-temperature diagenesis in shallow chalk reservoir, Skjold oil field, Danish North Sea: Evidence from fluid inclusions and oxygen isotopes. *American Association of Petroleum Geologists Bulletin*, **71**, 1378–1386.

Lindgreen, H., Drits, V.A., Sakharov, B.A., Jakobsen, H.J., Salyn, A.L., Dainyak, L.G., and Krøyer, H. (2002) The structure and diagenetic transformation of illite-smectite and chlorite-smectite from North Sea Cretaceous-Tertiary chalk. *Clay Minerals*, **37**, 429–450.

Maliva, R.G. and Dickson, J.A.D. (1994) Origin and environment of formation of late diagenetic dolomite in Cretaceous/Tertiary chalk, North Sea Central Graben. *Geological Magazine*, **131**, 609–617.

Maliva, R.G., Dickson, J.A.D., and Fallick, A.E. (1999) Kaolin cements in limestones: Potential indicators of organic-rich pore waters during diagenesis. *Journal of Sedimentary Research*, **69**, 158–163.

Mallon, A.J. and Swarbrick, R.E. (2002) A compaction trend for non-reservoir North Sea chalk. *Marine and Petroleum Geology*, **19**, 527–539.

Millot, G. (1970) *Geology of Clays*. Springer Verlag, New York, 429 pp.

Moore, D.M. and Reynolds, R.C. (1989) *X-ray Diffraction and the Identification and Analysis of Clay Minerals*. Oxford University Press, Oxford, UK, pp. 321–322.

Morgan, D.J. (1977) Simultaneous DTA-EGA of minerals and natural mineral admixtures. *Journal of Thermal Analysis*, **12**, 245–263.

Morse, J.W. and Mackenzie, F.T. (1990) *Geochemistry of Sedimentary Carbonates*. Developments in Sedimentology, **48**, Elsevier, Amsterdam, 707 pp.

Orton, R. and Unwin, P.R. (1993) Dolomite dissolution kinetics at low pH: A channel-flow study. *Journal of the Chemical Society – Faraday Transactions*, **89**, 3947–3954.

Pokrovsky, O.S. and Schott, J. (2002) Surface chemistry and dissolution kinetics of divalent metal carbonates. *Environmental Science and Technology*, **36**, 426–432.

Prieto, F.J.M. and Millero, F.J. (2002) The values of $pK_1 + pK_2$ for the dissociation of carbonic acid in seawater. *Geochimica et Cosmochimica Acta*, **66**, 2529–2540.

Rabinowicz, M., Dandurand, J.-L., Jabukowski, M., Schott, J., and Cassan, J.-P. (1985) Convection in a North Sea oil Reservoir: inferences on diagenesis and hydrocarbon migration. *Earth and Planetary Science Letters*, **74**, 387–404.

Reynolds, R.C. (1986) The Lorentz-polarization factor and preferred orientation in oriented clay aggregates. *Clays and Clay Minerals*, **34**, 359–367.

Safaricz, M. and Davison, I. (2005) Pressure solution in chalk. *American Association of Petroleum Geologists Bulletin*, **89**, 383–401.

Simonsen, L. and Toft, J. (2006) Texture, composition and stratigraphy of volcanic ash beds in lower Palaeocene chalk from the North Sea Central Graben area. *Marine and Petroleum Geology*, **23**, 767–776.

Taylor, S.R. and Lapré, J.F. (1987) North Sea chalk diagenesis: its effect on reservoir location and properties. Pp. 483–495 in: *Petroleum Geology of Northwest Europe: Proceedings of the 3rd Conference* (J. Brooks and K. Glennie, editors). Graham & Trotman, London.

Thiry, M. and Jacquin, T. (1993) Clay mineral distribution related to rift activity, sea-level changes and paleoceanography in the Cretaceous of the Atlantic Ocean. *Clay Minerals*, **28**, 61–84.

Warren, E.A., Smalley, P.C., and Howarth, R.J. (1994) Compositional variations of North Sea formation waters. Pp. 119–208 in: *North Sea Formation Waters Atlas* (E.A. Warren and P.C. Smalley, editors). Geological Society Memoir no. **15**. The Geological Society, London.

Webb, T.L. and Krüger, J.E. (1970) Carbonates. Pp. 303–342 in: *Differential Thermal Analysis*, **1**, (R.C. Mackenzie, editor). Academic Press, London.

Wray, D.S. (1995) Origin of clay-rich beds in Turonian chalks from Lower Saxony – a rare-earth element study. *Chemical Geology*, **119**, 161–173.

Wray, D.S. (1999) Identification and long-range correlation of bentonites in Turonian-Coniacian (Upper Cretaceous) chalks of northwest Europe. *Geological Magazine*, **136**, 361–371

Zhang, R., Hu, S., Zhang, X., and Yu, W. (2007) Dissolution kinetics of dolomite in water at elevated temperatures. *Aquatic Geochemistry*, **13**, 309–338.

(*Received 1 April 2008; revised 12 September 2008; Ms. 149; A.E. B. Lanson*)